

Coulomb breakup of ^{37}Mg and its ground state structure

Shubhchintak, Neelam, R. Chatterjee

Department of Physics, Indian Institute of Technology - Roorkee, 247667, India

R. Shyam

Theory Group, Saha Institute of Nuclear Physics, 1/AF Bidhannagar, Kolkata 700064, India, and Department of Physics, Indian Institute of Technology, Roorkee-247667, India

K. Tsushima

International Institute of Physics, Federal University of Rio Grande do Norte Av. Odilon Gomes de Lima, 1722 Capim Macio, Natal, RN 59078-400, Brazil

Abstract

We calculate Coulomb breakup of the neutron rich nucleus ^{37}Mg on a Pb target at the beam energy of 244 MeV/nucleon within the framework of a finite range distorted wave Born approximation theory that is extended to include the effects of projectile deformation. In this theory, the breakup amplitude involves the full wave function of the projectile ground state. Calculations have been carried out for the total one-neutron removal cross section (σ_{-1n}), the neutron-core relative energy spectrum, the parallel momentum distribution of the core fragment, the valence neutron angular, and energy-angular distributions. The calculated σ_{-1n} has been compared with the recently measured data to put constraints on the spin parity, and the one-neutron separation energy (S_n) of the ^{37}Mg ground state ($^{37}\text{Mg}_{gs}$). The dependence of σ_{-1n} on the deformation of this state has also been investigated. While a spin parity assignment of $7/2^-$ for the $^{37}\text{Mg}_{gs}$ is ruled out by our study, neither of the $3/2^-$ and $1/2^+$ assignments can be clearly excluded. Using the spectroscopic factor of one for both the $3/2^-$ and $1/2^+$ configurations and ignoring the projectile deformation effects, the S_n values

Email addresses: shub1dph@iitr.ac.in (Shubhchintak), nph10dph@iitr.ac.in (Neelam), rcfphfph@iitr.ac.in (R. Chatterjee), radhey.shyam@saha.ac.in (R. Shyam), kazuo.tsushima@gmail.com (K. Tsushima)

of 0.35 ± 0.06 MeV and 0.50 ± 0.07 MeV, respectively, are extracted for the two configurations. However, the extracted S_n is strongly dependent on the spectroscopic factor and the deformation effects of the respective configuration. The narrow parallel momentum distribution of the core fragment and the strong forward peaking of the valence neutron angular distribution suggest a one-neutron halo configuration in either of the $2p_{3/2}$ and $2s_{1/2}$ configurations of the ^{37}Mg ground state.

Keywords: Coulomb breakup of ^{37}Mg , deformation effects, one-neutron removal cross section, relative energy spectra, parallel momentum distributions, angular distributions

PACS: 24.10.Eq, 25.60.Gc, 27.30.+t

1. Introduction

With the advances made in the technology of producing nuclear species with relatively large neutron (N) to proton (Z) number ratios, it is now possible to extensively study nuclei near the neutron-drip line with $Z > 8$. During the last three decades measurements performed on mass, radius and spectroscopy of such nuclei have shown that they have structures that are at variance with those of their “near the line of stability” counterparts (see, e.g., [1, 2, 3, 4, 5, 6, 7, 8, 9, 10, 11, 12], and [13, 14, 15, 16, 17, 18, 19, 20, 21]). With the advent of new generation of radioactive ion beam facilities, it has now become possible not only to produce medium mass neutron rich nuclei in the vicinity of the magic numbers but also employ them as projectiles to initiate reactions (e.g., breakup) on nuclear targets [22, 23]. This provides excellent opportunity to perform quantitative study of the single-particle structure and the shell evolution in this region.

The notion of “magic” numbers is one of the most fundamental concepts in nuclear structure physics [24, 25]. If large gaps occur between groups of single-particle orbits that are completely filled with nucleons (neutrons or protons), then these nucleon numbers are called “magic”. The seven most established magic numbers are 2, 8, 20, 28, 50, 82, and 126. However, in several nuclei near the neutron-drip line, modifications to this shell structure have been observed [15]. In these cases the magic numbers evolve as a function of the neutron number - old magic numbers may disappear while new ones emerge and conventional shell gaps may break down. The region where abrupt onset of changes in the magic numbers appears, is called is-

land of inversion [26]. For example, rapid changes in nuclear structure and vanishing of the $N = 8$, and 20 shell gaps have been seen in neutron rich nuclei ^{12}Be [27], and ^{32}Mg [6] and $^{30,32}\text{Ne}$ [16], respectively. Examples of $N = 28$ shell quenching have been observed in $^{36,38}\text{Mg}$ [21] and ^{42}Si [28]. It is suggested in Ref. [26] that island of inversion near $N = 20, 28$ comes about because of the fact that the $\nu(sd)^{-2}(fp)^2$ intruder configurations (here ν represents a relative neutron state), in which two neutrons from the sd shell are excited to the fp shell, become so low in energy that they form the ground states for $Z = 10 - 12$ and $N = 20 - 22$ nuclei. This suggestion was confirmed subsequently by mass measurements of the neutron rich isotopes of Ne, Na and Mg nuclei [29]. Recently, this behavior has been shown to be a general phenomena that should occur for most standard shell closures far from the line of stability, and the mechanism behind this is found to be related to the importance of the nucleon-nucleon tensor interaction [30]. It is obvious that due to the intruder states, the single particle structure of the ground states of nuclei lying within island of inversion will not be the same as that emerging from the usual filling of the shell model states.

The mixing of neutron n-particle-n-hole ($np - nh$) intruder configurations of $\nu(sd)^{-n}(fp)^n$ character to the ground state, causes large deformation to nuclei in island of inversion near $N = 20, 28$, which is confirmed by the measured low excitation energies and $B(E2)$ values of the first excited states (see, eg., Refs. [3, 6, 8, 13, 16, 31]). It has been emphasized [26, 32, 33, 34] that the deformation may also account for the enhanced binding energies manifested in some of the known nuclei in this region. The collective properties of neutron rich nuclei near $N = 20$ region are rather well described by state-of-the-art Monte-Carlo shell model calculations that allow for unrestricted mixing of neutron particle-hole configurations across the shell gap [35, 36]. In Ref. [37, 38], nuclei in the neighborhood of neutron-drip line have been systematically investigated in a model where one-particle motion is described within spherical as well as deformed potentials. It has been concluded in this work that nuclei in the region of $N = 20 - 28$ are most likely to be deformed.

The root mean square radius (RMS) of a deformed nucleus becomes effectively larger than that of a spherical one. This enhances the total reaction cross section (σ_R) that depends on RMS radii of the projectile and the target nuclei. Large interaction cross sections (which are almost the same as the σ_R) have been measured for $^{29-32}\text{Ne}$ [39, 40] and $^{24-38}\text{Mg}$ [41] nuclei. This has led to the conclusion that the isotopes $^{29-32}\text{Ne}$ have strong deformation [42, 43, 44]. For the Mg case, these studies [44, 45] suggest that while

^{27}Mg and ^{30}Mg are spherical, $^{25,29,33-38}\text{Mg}$ are more likely to be deformed.

The discovery of halo structure in some of the drip line nuclei is another important progress made in the studies of nuclei with large N to Z ratio near the limits of nuclear stability [46, 47, 48, 49, 50, 51, 52]. As the neutron-drip line is approached nuclei experience weakening of the neutron binding energy, which leads to some special effects. The sudden rise of interaction cross sections with increasing N in some of these nuclei can be attributed to the extended density distribution(s) of the valence neutron(s). This decoupling of the valence neutron(s) from the tightly bound core and the extension of the corresponding wave function to much larger radii have been referred to as neutron halo. This phenomena has been seen earlier in lighter nuclei like ^{11}Li , ^{11}Be , ^{19}C [46].

In recent years, there has been considerable interest in finding out if halo configurations also exist in nuclei lying near the neutron-drip line in the vicinity of island of inversion [53, 54]. ^{31}Ne with $Z = 10$ and $N = 21$, is a promising candidate to have a one-neutron halo configuration because the one-neutron separation energy of this nucleus is quite small (0.29 ± 1.64 MeV [55], or 0.06 ± 0.41 MeV [56]). Indeed, such a structure has been suggested for this isotope by Coulomb breakup studies [22]. This has been further supported by measurements [39] of the interaction cross sections for Ne isotopes incident on a ^{12}C target at the beam energy of 240 MeV/nucleon, where it was found that for ^{31}Ne the interaction cross section was much larger than that of any other Ne isotope. Recently, measurements of σ_R for $^{24-38}\text{Mg}$ isotopes on ^{12}C target at the beam energy of 240 MeV/nucleon have been reported in Ref. [41]. From a similar reasoning, it was suggested in this study that ^{37}Mg ($Z = 12, N = 25$) that lies in $N = 20 - 28$ island of inversion, is also a candidate for having a one-neutron halo structure. This was reinforced by measurements of Coulomb breakup of ^{37}Mg on C and Pb targets at the beam energy of 244 MeV/nucleon in Ref. [23].

The observation of the halo phenomena in the heavier nuclei lying in island of inversion, signals major changes in the shell evolution in these nuclei as compared to that seen in the spherical ones. One of the conditions for the halo formation is that the loosely bound neutron in the nucleus occupies a low orbital angular momentum state ($\ell = 0$ or 1) in order to reduce the centrifugal barrier effects that prevent it from spreading out [53]. In fact, in well established cases of light one-neutron halo nuclei like ^{11}Be and ^{19}C , the ground states have predominant s -wave neutron plus core configurations [49, 57, 58, 59, 60]. According to the conventional shell model evolution,

one expects to see the domination of the $1f_{7/2}$ orbit in nuclei in the vicinity of $N = 20 - 28$. This would not favor the halo formation because a larger centrifugal barrier would prevent the $l = 3$ neutrons to extend too far out in the space. Therefore, a significant contribution from the s - or p -wave orbits has to be there in the ground state structure of these nuclei to minimize the centrifugal barrier. Thus, the existence of halo structure would imply a significant modification of the shell structure that involves considerable mixing of the intruder states like $2p_{3/2}$ or $2s_{1/2}$ into the ground states of these nuclei, which also leads to the appreciable deformation of these states. Therefore, the halo formation in heavier nuclei in island of inversion region has strong correlation with the shell evolution and the presence of deformation.

Coulomb breakup reaction, in which the valence neutron is removed from the fast projectile in Coulomb fields of heavy target nuclei, provides a convenient tool to investigate the halo structure in the neutron-drip line nuclei (see, e.g., the review [62]). It places constraints on their electric dipole response [57, 61, 62]. A class of theories of this reaction (e.g., the post form finite range distorted wave Born approximation (FRDWBA) theory [49, 63]) requires realistic wave functions to describe the relative motion between the valence neutron and the core in the ground state of the projectile. Thus by comparing the calculations of the cross sections with the measured data, one can directly probe the ground state structure of the projectile. Narrow widths of the parallel momentum distributions of the core fragments provide a robust signature of the presence of halo structure in the projectile nuclei as they imply a larger spatial spread of the fragments in their ground states.

Recently [64], the FRDWBA theory of Coulomb breakup reactions has been extended to include the deformation of the projectile by using a deformed Woods-Saxon potential to describe the valence neutron-core relative motion. Hence, this provides a microscopic theoretical tool to study the Coulomb breakup of neutron-drip line nuclei lying in island of inversion in the vicinity of $N = 20 - 28$ and to investigate the correlation between halo formation and the shell evolution and deformation. In the first application of this theory, the Coulomb breakup of ^{31}Ne on a Pb target at the beam energy of 234 MeV/nucleon was investigated [64]. Comparison of calculated and the measured σ_{-1n} (of Refs. [22, 65]) suggested that the ground state of ^{31}Ne is most likely to have a $^{30}\text{Ne} \otimes 2p_{3/2}\nu$ configuration. The value of the one-neutron separation energy S_n is found to be correlated to the quadrupole deformation parameter (β_2). For β_2 between 0.0 - 0.5, S_n varies between 0.24 - 0.58 MeV. The calculated full width at half maximum (FWHM) of

the parallel momentum distribution of ^{30}Ne fragment is closer to that of the core fragment seen in the breakup reaction of the established halo nucleus ^{11}Be . This strongly suggests that the ground state of ^{31}Ne has a one-neutron halo structure in the $2p_{3/2}$ state.

^{37}Mg is the most neutron-rich bound odd-mass Mg isotope. However, the experimental information about its mass and the ground state spin parity is not available, even though mass systematics suggest that it is a very weakly bound system with S_n in the range of 0.16 ± 0.68 MeV [66]. Therefore, it is another promising candidate for having a one-neutron halo structure in island of inversion near $N = 20 - 28$. However, a $1f_{7/2}$ configuration for its ground state that would result in the conventional spherical shell model, will suppress the halo formation due to the high centrifugal barrier. Hence, a significant modification of its spherical shell structure with introduction of the intruder configurations having s - and p -wave states, is necessary for this nucleus to have a halo like structure. This also implies that its ground state should be deformed.

The aim of this paper is to investigate the one-neutron removal cross section of ^{37}Mg on a Pb target at the beam energy of 244 MeV/nucleon within the FRDWBA theory of Coulomb breakup reactions. By comparing the σ_{-1n} calculated within this theory with the corresponding experimental data we would like to extract most plausible spin parity for the ground state of this nucleus. We attempt to put constraints on the large uncertainty in its S_n value. We investigate the effect of the ground state deformation of this nucleus on the values of σ_{-1n} deduced in our analysis. Furthermore, we make predictions for the observables such as relative energy spectra of the valence neutron-core fragments, parallel momentum distribution of the core fragment, and the angular distribution of the valence neutron as a function of deformation. Our study is expected to provide more understanding about the evolution of the shell structure in island of inversion from $N = 20$ to 28, about which some conflicting results have been reported recently [13, 21]. Furthermore, our study is expected to quantify the presence of a neutron halo structure in ^{37}Mg and provide information about its correlation to the ground state deformation of this nucleus.

The study of Coulomb breakup of ^{37}Mg is also of interest in astrophysics because it provides an indirect way to determine the rate of the radiative neutron capture reaction $^{36}\text{Mg}(n, \gamma)^{37}\text{Mg}$, which is of importance in the study of the r -process nucleosynthesis in supernovae [67].

In the next section, we present our formalism where we recall some impor-

tant aspects of the FRDWBA theory of breakup reactions and its extension to include the deformation of the projectile ground state. The results of our calculations are presented in section 3, where we discuss the one-neutron removal cross section, the relative energy spectra of the fragments, the parallel momentum distribution of the core fragment, the angular and energy distribution of valence neutron as a function of the projectile deformation. The summary and conclusions of our study are presented in section 4.

2. Formalism

The breakup reaction of a projectile a into the core fragment b and the valence neutron n , in the Coulomb field of a target t can be represented as $a + t \rightarrow b + n + t$. We assume that target nucleus remains in its ground state during the breakup process. Thus this is also known as the elastic breakup reaction. The chosen coordinate system is shown in Fig. 1. The position

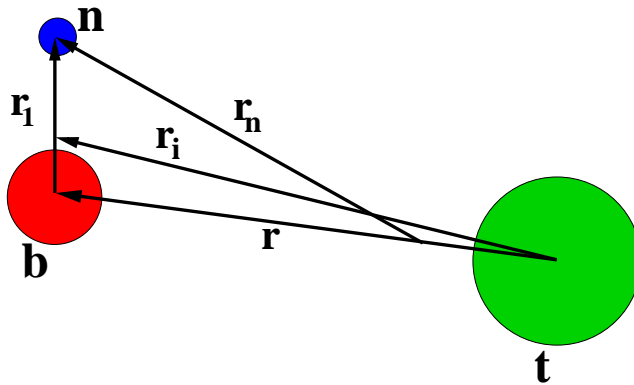


Figure 1: The three-body coordinate system. The charged core fragment, the valence neutron and the target nucleus are denoted by b , n and t , respectively.

vectors satisfy the following relations:

$$\mathbf{r} = \mathbf{r}_i - \alpha \mathbf{r}_1, \quad \alpha = \frac{m_n}{m_n + m_b}, \quad (1)$$

$$\mathbf{r}_n = \gamma \mathbf{r}_1 + \delta \mathbf{r}_i, \quad \delta = \frac{m_t}{m_b + m_t}, \quad \gamma = (1 - \alpha\delta). \quad (2)$$

The starting point of the FRDWBA theory of Coulomb breakup is the

post-form T -matrix of the reaction given by

$$T = \int d\xi d\mathbf{r}_1 d\mathbf{r}_i \chi_b^{(-)*}(\mathbf{k}_b, \mathbf{r}) \Phi_b^*(\xi_b) \chi_n^{(-)*}(\mathbf{k}_n, \mathbf{r}_n) \Phi_n^*(\xi_n) V_{bn}(\mathbf{r}_1) \Psi_a^{(+)}(\xi_a, \mathbf{r}_1, \mathbf{r}_i). \quad (3)$$

The functions χ are the distorted waves for the relative motions of b and n with respect to t and the center of mass (c.m.) of the $b+t$ system, respectively. The functions Φ are the internal state wave functions of the concerned particles dependent on the internal coordinates ξ . The function $\Psi_a^{(+)}(\xi_a, \mathbf{r}_1, \mathbf{r}_i)$ is the exact three-body scattering wave function of the projectile with a wave vector \mathbf{k}_a satisfying outgoing boundary conditions. The vectors \mathbf{k}_b and \mathbf{k}_n are the Jacobi wave vectors of b and n , respectively, in the final channel of the reaction. The function $V_{bn}(\mathbf{r}_1)$ represents the interaction between b and n . As we concentrate only on Coulomb breakup, the function $\chi_b^{(-)}(\mathbf{k}_b, \mathbf{r})$ is taken as the Coulomb distorted wave (for a point Coulomb interaction between the charged core b and the target) satisfying incoming wave boundary conditions, and the function $\chi_n^{(-)}(\mathbf{k}_n, \mathbf{r}_n)$ describing the relative motion of the neutron with respect to the target, is just a plane wave. It may be noted that within this approach the fragment-target interactions are treated to all orders.

In the distorted wave Born approximation (DWBA), we write

$$\Psi_a^{(+)}(\xi_a, \mathbf{r}_1, \mathbf{r}_i) = \Phi_a(\xi_a, \mathbf{r}_1) \chi_a^{(+)}(\mathbf{k}_a, \mathbf{r}_i), \quad (4)$$

The assumption inherent in Eq. (4) is that the breakup channels are very weakly coupled and hence this coupling needs to be treated only in the first order. We expect this approximation to be valid for those cases where there are no resonances in the $n + b$ continuum. Most of the neutron halo systems come in this category. For those cases where higher order effects of fragment-fragment interaction are non-negligible, the applicability of this method would be limited. Ideally, a rigorous description of the breakup process of all types of projectiles would require the use of Faddeev type of three-body methods that include Coulomb potentials in the fragment-target and fragment-fragment (if required) interactions. A few such calculations have become available recently although they are confined to the breakup reactions on a proton target [68, 69, 70, 71].

In Eq. (4) the dependence of Φ_a on \mathbf{r}_1 describes the relative motion of the fragments b and n in the ground state of the projectile. The function $\chi_a^{(+)}(\mathbf{k}_a, \mathbf{r}_i)$ is the Coulomb distorted scattering wave describing the relative

motion of the c.m. of the projectile with respect to the target, satisfying outgoing wave boundary conditions.

The integration over the internal coordinates ξ in the T -matrix gives

$$\int d\xi \Phi_b^*(\xi_b) \Phi_n^*(\xi_n) \Phi_a(\xi_a, \mathbf{r}_1) = \sum_{\ell m j \mu} \langle \ell m j_n \mu_n | j \mu \rangle \langle j_b \mu_b j \mu | j_a \mu_a \rangle i^\ell \Phi_a(\mathbf{r}_1) \quad (5)$$

The wave function $\Phi_a(\mathbf{r}_1)$ can be expressed in terms of its radial and angular parts assuming a particular partition, in which the relative motion between n and b has an orbital angular momentum ℓ as

$$\Phi_a(\mathbf{r}_1) = \sqrt{C^2 S} u_\ell(r_1) Y_\ell^m(\hat{\mathbf{r}}_1), \quad (6)$$

where $C^2 S$ is the spectroscopic factor for the given partition. In Eq. (5), ℓ is coupled to the spin of n and the resultant channel spin j is coupled to the spin j_b of the core b to yield the spin of a (j_a). The partition represented by Eq. (6) will be retained even if the potential $V_{bn}(\mathbf{r}_1)$ is deformed.

The T -matrix can now be written as

$$T = \sum_{\ell m j \mu} \langle \ell m j_n \mu_n | j \mu \rangle \langle j_b \mu_b j \mu | j_a \mu_a \rangle i^\ell \hat{\ell} \beta_{\ell m}(\mathbf{k}_b, \mathbf{k}_n; \mathbf{k}_a), \quad (7)$$

where

$$\begin{aligned} \hat{\ell} \beta_{\ell m}(\mathbf{k}_b, \mathbf{k}_n; \mathbf{k}_a) &= \int d\mathbf{r}_1 d\mathbf{r}_i \chi_b^{(-)*}(\mathbf{k}_b, \mathbf{r}) e^{-i\mathbf{k}_n \cdot \mathbf{r}_n} \\ &\times V_{bn}(\mathbf{r}_1) u_\ell(r_1) Y_\ell^m(\hat{\mathbf{r}}_1) \chi_a^{(+)}(\mathbf{k}_a, \mathbf{r}_i). \end{aligned} \quad (8)$$

with $\beta_{\ell m}$ being the reduced T -matrix and with $\hat{\ell} \equiv \sqrt{2\ell + 1}$.

Eq. (8) involves a six dimensional integral which makes the computation of $\beta_{\ell m}$ quite complicated. The problem gets further acute because the integrand involves a product of three scattering waves that exhibit oscillatory behavior asymptotically. In the past calculations have been simplified by using approximate methods, such as the zero-range approximation (see e.g., [72, 73, 74]) or the Baur-Trautmann approximation [75, 76] that led to the factorization of the T -matrix into two terms; each involving three-dimensional integrals (we refer to [77] for a detailed discussion). However, these methods are not valid for breakup reactions at higher beam energies and for heavier projectiles that can have non- s -wave ground states.

In our FRDWBA theory we use a method that was proposed in Ref. [78] for describing the heavy ion induced transfer reactions, and was adopted in Ref. [79] for describing the breakup reactions of heavy projectiles. This was shown [63, 77] to be well suited for calculating the Coulomb breakup of halo nuclei. In this method, the Coulomb distorted wave of particle b in the final channel is written as [63]

$$\chi_b^{(-)}(\mathbf{k}_b, \mathbf{r}) = e^{-i\alpha\mathbf{K}\cdot\mathbf{r}_1} \chi_b^{(-)}(\mathbf{k}_b, \mathbf{r}_i). \quad (9)$$

Eq. (9) represents an exact Taylor series expansion about \mathbf{r}_i if $\mathbf{K} = -i\nabla_{\mathbf{r}_i}$ is treated exactly. However, instead of doing this we employ a local momentum approximation (LMA) where the magnitude of momentum \mathbf{K} is taken to be

$$K(\mathcal{R}) = \sqrt{\frac{2m}{\hbar^2}(E - V(\mathcal{R}))}. \quad (10)$$

Here m is the reduced mass of the $b-t$ system, E is the energy of particle b relative to the target in the c.m. system and $V(\mathcal{R})$ is the Coulomb potential between b and the target separated by \mathcal{R} . Thus, the magnitude of the momentum of \mathbf{K} is evaluated at some separation \mathcal{R} , which is held fixed for all the values of r . The value of \mathcal{R} was taken to be equal to 10 fm. For reactions under investigation in this paper, the magnitude of \mathbf{K} remains constant for distances larger than 10 fm. Due to the peripheral nature of the breakup reaction, the region $\mathcal{R} \gtrsim 10$ fm contributes maximum to the cross section. Furthermore, the results of the calculations for these reactions, at the beam energies under investigation, are almost independent of the choice of the direction of momentum \mathbf{K} [63]. Therefore, we have taken the directions of \mathbf{K} and \mathbf{k}_b to be the same in all the calculations presented in this paper.

Substituting Eq. (9) into Eq. (8), the reduced amplitude is obtained in a factorized form as

$$\begin{aligned} \hat{\ell}\beta_{\ell m} &= \int d\mathbf{r}_i e^{-i\delta\mathbf{q}_n\cdot\mathbf{r}_i} \chi_b^{(-)*}(\mathbf{q}_b, \mathbf{r}_i) \chi_a^{(+)}(\mathbf{q}_a, \mathbf{r}_i) \\ &\times \int d\mathbf{r}_1 e^{-i\mathbf{Q}\cdot\mathbf{r}_1} V_{bn}(\mathbf{r}_1) u_\ell(r_1) Y_\ell^m(\hat{\mathbf{r}}_1), \end{aligned} \quad (11)$$

where, $\mathbf{Q} = \gamma\mathbf{q}_n - \alpha\mathbf{K}$. The first integral in Eq. (11), is the dynamics part in the Coulomb breakup and is expressed analytically in terms of the Bremsstrahlung integral [80]. The second integral in Eq. (11) contains the projectile structure information.

We now introduce deformation in potential $V_{bn}(\mathbf{r}_1)$ in Eq. (11). Following [81], we write the axially symmetric quadrupole-deformed Woods-Saxon potential (without taking the spin-orbit term) as

$$V_{bn}(\mathbf{r}_1) = V_{ws}(r_1) - \beta_2 k(r_1) Y_2^0(\hat{\mathbf{r}}_1). \quad (12)$$

We take the Woods-Saxon form for the potential $V_{ws}(r_1)$, and write, $V_{ws}(r_1) = V_{ws}^0 f(r_1)$, where V_{ws}^0 is the depth of the potential and $f(r_1)$ describes its shape. $f(r_1)$ and $k(r_1)$ are defined as

$$f(r_1) = \frac{1}{1 + \exp(\frac{r_1 - R}{a})}, \quad k(r_1) = RV_{ws}^0 \frac{df(r_1)}{dr_1},$$

with radius $R = r_0 A^{1/3}$ where r_0 and a are the radius and diffuseness parameters, respectively. β_2 is the quadrupole deformation parameter. In Eq. (12), we have included only the lowest-order term in the deformation parameter of the deformed Woods-Saxon potential (see, e.g., Ref. [82]). This is an approximation. However, this should be sufficient for our purpose of illustrating the role of projectile deformation effects on the breakup cross sections.

The radial wavefunction corresponding to the potential $V_{bn}(\mathbf{r}_1)$ should be obtained by solving the coupled equation

$$\begin{aligned} & \left\{ \frac{d^2}{dr_1^2} - \frac{\ell(\ell+1)}{r_1^2} + \frac{2\mu}{\hbar^2} [E - V_{ws}(r_1)] \right\} u_{\ell m}(r_1) \\ &= \frac{2\mu}{\hbar^2} \sum_{\ell'} \langle Y_\ell^m(\hat{\mathbf{r}}_1) | -\beta_2 k(r_1) Y_2^0(\hat{\mathbf{r}}_1) | Y_{\ell'}^m(\hat{\mathbf{r}}_1) \rangle u_{\ell' m}(r_1). \end{aligned} \quad (13)$$

Therefore, the radial wave functions obtained from Eq. (13), corresponding to a given ℓ will have an admixture of wave functions corresponding to other ℓ values of the same parity. Thus this wave function can be quite different from that of the spherical Woods-saxon potential. However, if components of the admixed states of higher ℓ are quite weak, then the pure states of lowest ℓ can become dominant. In such a situation, one can use the solutions of the spherical Woods-Saxon potential corresponding to a single ℓ for the wave function $u_\ell(r_1)$ in Eq. (11). Indeed, it has been shown in Ref. [81] that as the binding energies approach zero, the lowest ℓ components become dominant in the neutron orbits of the realistic deformed potential irrespective of the size of the deformation. In this work, we have made the approximation of taking $u_\ell(r_1)$ as the state of a given single ℓ value that is the solution of the

Schrödinger equation with spherical Woods-Saxon potential. In any case, if the spectroscopic factors of shell model calculations are used for a particular state, the wave functions obtained in a spherical basis for that state should already include the admixture of different ℓ states.

We would like to point out here that only the structure part of the amplitude given by Eq. (11) is affected by the deformation in the interaction $V_{bn}(\mathbf{r}_1)$ - the dynamical part of it remains the same as it would be in no-deformation case. With the deformation effects introduced through Eq. (12), analytic expressions can be written for the structure part of the amplitude in Eq. (11). Let us define

$$I_f = \int d\mathbf{r}_1 e^{-i\mathbf{Q}\cdot\mathbf{r}_1} V_{bn}(\mathbf{r}_1) u_\ell(r_1) Y_\ell^m(\hat{\mathbf{r}}_1). \quad (14)$$

We can write (see, Ref. [64] for details of this derivation),

$$I_f = 4\pi \sum_{l_1 m_1} i^{-l_1} Y_{l_1}^{m_1}(\hat{\mathbf{Q}}) \int r_1^2 dr_1 j_{l_1}(Qr_1) u_\ell(r_1) \times \left[V_{ws}(r_1) \delta_{l_1, \ell} \delta_{m_1, m} - \beta_2 R V_{ws}^0 \frac{df(r_1)}{dr_1} I_1 \right], \quad (15)$$

where I_1 is defined as

$$I_1 = \int d\Omega_{r_1} Y_2^0(\hat{\mathbf{r}}_1) Y_{l_1}^{m_1*}(\hat{\mathbf{r}}_1) Y_\ell^m(\hat{\mathbf{r}}_1) = (-1)^{m_1} \sqrt{\frac{5}{4\pi}} \left[\frac{(2\ell+1)(2l_1+1)}{4\pi} \right]^{1/2} \times \begin{pmatrix} l_1 & 2 & \ell \\ 0 & 0 & 0 \end{pmatrix} \begin{pmatrix} l_1 & 2 & \ell \\ -m_1 & 0 & m \end{pmatrix}, \quad (16)$$

with $|\ell-2| < l_1 < |\ell+2|$ and $m_1 = m$. Notice that there would be a limited number of l_1 values to be considered, given that ℓ is the orbital angular momentum of the projectile ground state. In the limit of $\beta_2 = 0$, the above equation would contain the first term in the square bracket [involving the spherical potential $V_{ws}(r_1)$] that is reduced precisely in the same form as that obtained in Ref. [63] for the case where there is no deformation.

In Eq. (14), the spherical harmonic $Y_{l_1}^{m_1*}(\hat{\mathbf{Q}})$ (where $\mathbf{Q} = \gamma\mathbf{q}_n - \alpha\mathbf{K}$) can be written in terms of product of two spherical harmonics, one depending on $\hat{\mathbf{q}}_n$ and the other depending on $\hat{\mathbf{K}}$, using Moshinsky's formula [83]:

$$(|\mathbf{Q}|)^{l_1} Y_{l_1}^{m_1}(\hat{\mathbf{Q}}) = \sum_{LM_L} \frac{\sqrt{4\pi}}{\hat{L}} \begin{pmatrix} 2l_1+1 \\ 2L \end{pmatrix}^{1/2} |\alpha K|^{l_1-L} (\gamma q_n)^L$$

$$\times \langle l_1 - L \ m_1 - M_L \ L \ M_L | l_1 \ m_1 \rangle Y_{l_1-L}^{m_1-M}(\hat{\mathbf{K}}) Y_L^M(\hat{\mathbf{q}}_n), \quad (17)$$

where $\binom{2l_1+1}{2L}$ is the binomial coefficient and $\hat{L} = \sqrt{2L+1}$ with L varying from 0 to l_1 . Therefore, the structure part Eq. (15), can be evaluated and would contain the effect of the deformation of the projectile.

We once again wish to emphasize the analytic nature of our calculation at this point. With the structure part given by Eq. (15), the dynamics part in Eq. (11) is still given by the Bremsstrahlung integral, which can be solved analytically.

The triple differential cross section for the reaction is related to reduced transition amplitude $\beta_{\ell m}$ as

$$\frac{d^3\sigma}{dE_b d\Omega_b d\Omega_n} = \frac{2\pi}{\hbar v_a} \rho(E_b, \Omega_b, \Omega_n) \sum_{\ell m} |\beta_{\ell m}|^2, \quad (18)$$

where v_a is the $a-t$ relative velocity in the entrance channel and $\rho(E_b, \Omega_b, \Omega_n)$ is the phase space factor appropriate to the three-body final state.

3. Results and discussions

The formalism described in Section 2, has been employed to investigate Coulomb breakup of ^{37}Mg on a Pb target at the beam energy of 244 MeV/nucleon. In our analysis the calculated one-neutron removal cross sections are compared with the corresponding data as reported in Ref. [23]. To calculate the Coulomb breakup amplitude [see, Eq. (11)], we require the single-particle wave function $u_\ell(r)$ that describes the core-valence neutron relative motion in the ground state of the projectile (for a given neutron-core configuration). As discussed in the previous section, we take this wave function as that of a state of a single ℓ value and obtain it by solving the Schrödinger equation with a spherical Woods-Saxon potential with radius (r_0) and diffuseness (a) parameters of 1.24 fm and 0.62 fm, respectively. The depth of this well is adjusted to reproduce the valence neutron separation energy corresponding to this state.

Various observables for the reaction have been obtained by integrating the triple differential cross sections [see, Eq. (17)] over appropriate angles and energies of the unobserved quantity. For example, the total Coulomb

Table 1: Depth (V_{ws}^0) of the Woods-Saxon potential well as a function of S_n corresponding to neutron removal from the $2p_{3/2}$, $2s_{1/2}$, $1f_{7/2}$ orbitals. The values of parameters r_0 and a are taken to be 1.24 fm and 0.62 fm, respectively in all the cases.

S_n (MeV)	V_{ws}^0 ($2p_{3/2}$) (MeV)	V_{ws}^0 ($2s_{1/2}$) (MeV)	V_{ws}^0 ($1f_{7/2}$) (MeV)
0.01	43.97	24.73	43.36
0.05	44.18	25.28	43.43
0.10	44.42	25.72	43.53
0.15	44.64	26.06	43.62
0.20	44.84	26.36	43.71
0.22	44.92	26.47	43.75
0.25	45.04	26.63	43.81
0.30	45.23	26.88	43.90
0.35	45.42	27.11	43.99
0.40	45.60	27.33	44.09
0.45	45.77	27.53	44.18
0.50	45.94	27.73	44.27
0.55	46.11	27.92	44.37
0.60	46.28	28.11	44.46
0.65	46.44	28.29	44.55
0.70	46.60	28.46	44.64

one-nucleon removal cross section for a given ℓj configuration of the valence neutron is obtained by integrating the triple differential cross sections over angles and energy of fragment b and angles of the valence neutron n .

The nuclei in island of inversion are expected to have significant components of $2p - 2h$ [$\nu(sd)^{-2}(fp)^2$] neutron intruder configurations. Indeed, in Ref. [23], it has been argued that the valence neutron in $^{37}\text{Mg}_{g.s}$ is most likely to have a spin parity (J^π) of $3/2^-$ that corresponds to the $2p_{3/2}$ orbital. In this work, we have considered neutron removal from the $2p_{3/2}$, $2s_{1/2}$ and $1f_{7/2}$ orbitals that correspond to ^{37}Mg ground state J^π of $3/2^-$, $1/2^+$, and $7/2^-$, respectively. Since the S_n of the valence neutron in the ^{37}Mg ground state is still uncertain, we show in Table 1, values of the depths of the potential well as a function of S_n for all of the three orbitals.

In Fig. 2, we present the results of our calculations for the pure Coulomb

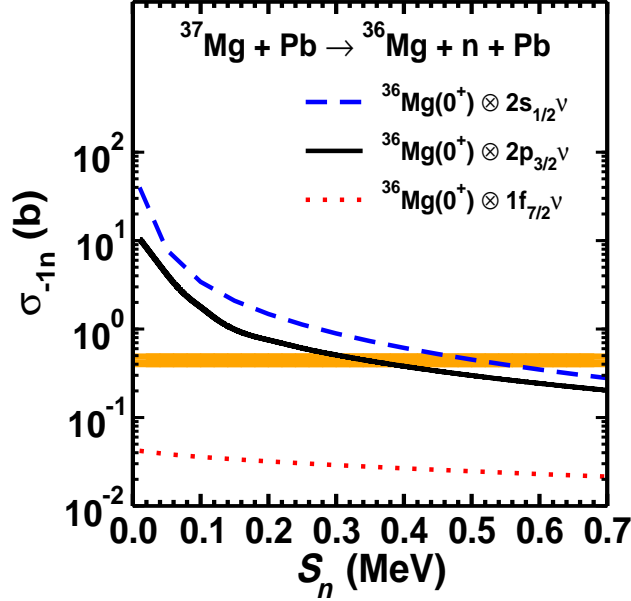


Figure 2: Pure Coulomb total one-neutron removal cross section, σ_{-1n} , in the breakup reaction of ^{37}Mg on a Pb target at 244 MeV/nucleon beam energy as a function of one-neutron separation energy S_n obtained with configurations $^{36}\text{Mg}(0^+) \otimes 2p_{3/2}\nu$ (solid line), $^{36}\text{Mg}(0^+) \otimes 2s_{1/2}\nu$ (dashed line) and $^{36}\text{Mg}(0^+) \otimes 1f_{7/2}\nu$ (dotted line) for $^{37}\text{Mg}_{gs}$ using the spectroscopic factors (C^2S) 1.0 in each case. The experimental cross section (taken from Ref. [23]) is shown by the shaded band.

σ_{-1n} in the breakup reaction of ^{37}Mg on a Pb target at the beam energy of 244 MeV/nucleon as a function of S_n corresponding to the one-neutron removal from the $2p_{3/2}$, $2s_{1/2}$ and $1f_{7/2}$ orbitals. For C^2S we have used a uniform value of one for each configuration. The shaded band in this figure shows the corresponding measured cross section taken from Ref. [23] with its width representing the experimental uncertainty. We note that calculated cross sections obtained with the $^{36}\text{Mg}(0^+) \otimes 2p_{3/2}\nu$ and $^{36}\text{Mg}(0^+) \otimes 2s_{1/2}\nu$ configurations (solid and dashed lines, respectively in Fig. 2) overlap with the experimental band in the S_n regions of 0.35 ± 0.06 MeV and 0.50 ± 0.07 MeV, respectively. Theoretical cross sections for the $2p_{1/2}$ case are almost identical to those of the $2p_{3/2}$ case. On the other hand, for the $^{36}\text{Mg}(0^+) \otimes 1f_{7/2}\nu$ configuration there is no overlap between calculated and experimental cross sections anywhere, which excludes the assignment of $J^\pi = 7/2^-$ to $^{37}\text{Mg}_{gs}$. Therefore, our results are consistent with the assignment of either of the $3/2^-$ and $1/2^+$ spin parity to the ground state of ^{37}Mg with one-neutron separation

energies in the ranges as stated above. The S_n deduced in our work for either of these configurations is within the range of the evaluated value of 0.16 ± 0.68 MeV as reported in the most recent nuclear mass tabulation [66].

Nevertheless, it should be noted that there is a wide variation in the C^2S values for these states reported in the literature. For $^{36}\text{Mg}(0^+) \otimes 2p_{3/2}\nu$ and $^{36}\text{Mg}(0^+) \otimes 2s_{1/2}\nu$ configurations, while the shell model C^2S values are reported to be 0.31 and 0.001, respectively [35], values extracted from an analysis of the ^{37}Mg breakup data [23] are $0.42^{+0.14}_{-0.12}$ and $0.40^{+0.16}_{-0.13}$, respectively. In the latter work the theoretical cross sections have been computed from the eikonal model of Ref. [84] for the C target and from the (semiclassical) Coulomb breakup model of Ref. [65] for the Pb target. On the other hand, for the $^{36}\text{Mg}(0^+) \otimes 1f_{7/2}\nu$ configuration the C^2S is not mentioned in these references. For a given neutron-core configuration S_n extracted from the Coulomb breakup data is intimately related to the value of C^2S . Therefore, it would be interesting to investigate the C^2S dependence of S_n extracted in our study.

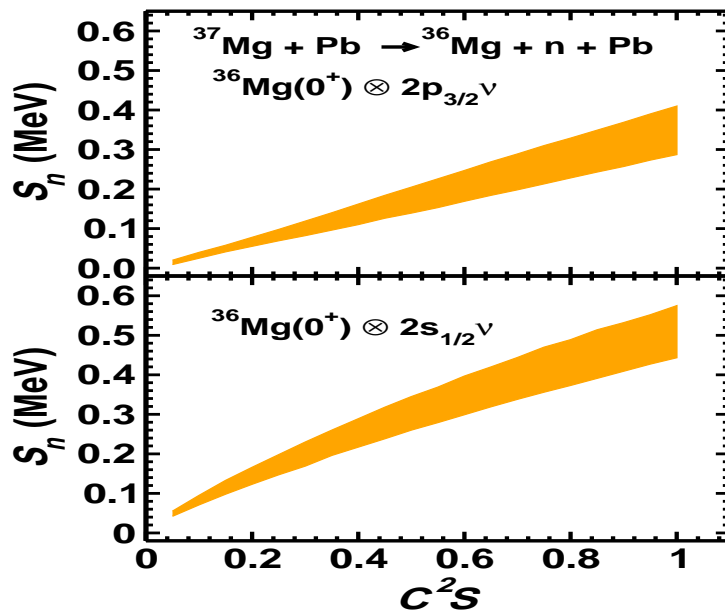


Figure 3: (a) S_n as a function of C^2S for the same reaction as in Fig. 2 with the $^{37}\text{Mg}_{gs}$ configuration of $^{36}\text{Mg}(0^+) \otimes 2p_{3/2}\nu$, (b) same as in (a) for the $^{36}\text{Mg}(0^+) \otimes 2s_{1/2}\nu$ configuration

In Figs. 3(a) and 3(b), we show this correlation for the same reaction as in

Fig. 2 for the configurations $^{36}\text{Mg}(0^+) \otimes 2p_{3/2}\nu$ and $^{36}\text{Mg}(0^+) \otimes 2s_{1/2}\nu$ of the $^{37}\text{Mg}_{gs}$, respectively. In these calculations, for each C^2S the corresponding S_n is deduced from the region of overlap of the calculated cross section and the measured data band as shown in Fig. 2. We see that S_n increases steadily with increasing C^2S . Also the uncertainty in the extracted S_n increases with C^2S , because at larger C^2S flatter portions of the calculated cross section overlap with the data band that encompasses larger parts of the band. It may be mentioned here that in our calculations S_n corresponding to the C^2S of 0.42 for the configuration $^{36}\text{Mg}(0^+) \otimes 2p_{3/2}\nu$, is 0.14 ± 0.03 MeV, which is lower than the mean value of S_n (0.22 MeV) obtained in Ref. [23] for the same C^2S . It is clear from this figure that for a reliable extraction of S_n from the Coulomb breakup studies, it is essential to have accurate knowledge of the spectroscopic factors for different configurations.

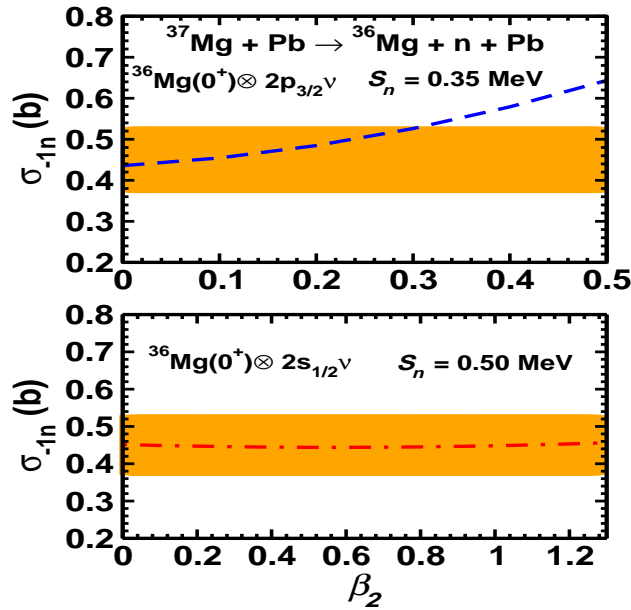


Figure 4: (a) σ_{-1n} as a function of the deformation parameter β_2 in the Coulomb breakup of ^{37}Mg on a Pb target at the beam energy of 244 MeV/nucleon with the configuration $^{36}\text{Mg}(0^+) \otimes 2p_{3/2}\nu$ for $^{37}\text{Mg}_{gs}$. The S_n is taken to be 0.35 MeV with C^2S values being 1.0. (b) Same as in Fig. (a) for $^{36}\text{Mg}(0^+) \otimes 2s_{1/2}\nu$ configuration with C^2S and S_n of 1.0 and 0.50 MeV, respectively. In both (a) and (b) the experimental data (shown by the shaded region) are taken from Ref. [23].

To substantiate the information extracted from the studies of the one-neutron removal cross section, it is desirable to investigate other effects and

observables to determine the most reliable configuration of $^{37}\text{Mg}_{gs}$. To this end, in Figs. 4(a) and 4(b) we investigate the effect of projectile deformation on σ_{-1n} for the reaction studied in Fig. 2. As discussed earlier, the presence of neutrons in nearby degenerate j shells (eg., $1f_{7/2}$ and $2p_{3/2}$) in ^{37}Mg that couple strongly to each other by the quadrupole-quadrupole interaction, can lead to the quadrupole deformation of this nucleus.

In Fig. 4(a), we show our results for σ_{-1n} as a function of β_2 for the $^{36}\text{Mg}(0^+) \otimes 2p_{3/2}\nu$ configuration of $^{37}\text{Mg}_{gs}$ with C^2S values of 1.0 corresponding to a S_n of 0.35, which is the mean value of the one-neutron separation energies extracted from the comparison of the calculated and experimental total cross sections in Fig. 2. For $\beta_2 = 0$, the σ_{-1n} is the same as that shown in Fig. 2 for the same value of S_n . With increasing β_2 , the cross section increases, and the overlap between calculations and the data band ceases for $\beta_2 > 0.32$. Therefore, our calculations do not support a quadrupole deformation parameter in excess of 0.32 for this state.

In Fig. 4(b) we show the same results for the $^{36}\text{Mg}(0^+) \otimes 2s_{1/2}\nu$ configuration with C^2S and S_n values of 1.0 and 0.50 MeV, respectively, The contribution of the deformation term to the cross section is substantially low for the s -wave configuration, which results in almost constant σ_{-1n} as a function of β_2 as seen in Fig. 4(b). We further note that in contrast to the results in Fig. 4(a), the overlap between calculated cross sections and the data band exists even for values of β_2 as high as 1.2. We have checked that the situation remains the same for β_2 values even beyond 1.2. This result indicates that the s -wave configuration does not provide any constraint on the deformation parameter β_2 in our calculations. On the other hand, the Nilsson model study of Ref. [37] predicts the β_2 parameter of the $2s_{1/2}$ state to be below 0.3. This, however, does not imply that the s -wave configuration is negated for the ground state of ^{37}Mg in our calculations. It simply does not constrain the β_2 value for this state. In any case, it is not possible to obtain more definite constraints on the configuration of $^{37}\text{Mg}_{gs}$ from a single measurement as available at present.

The variation of S_n with the deformation parameter β_2 is studied in Fig. 5 for the same reaction as in Fig. 4(a) for the $^{37}\text{Mg}_{gs}$ configuration of $^{36}\text{Mg}(0^+) \otimes 2p_{3/2}\nu$ with C^2S value of one. Several authors have argued that the deformation can lead to the enhancement of binding energies in the island of inversion region nuclei [32, 26, 34, 85] due to the mixing of $2\hbar\omega$ $2p - 2h$ neutron excitations to $0\hbar\omega$ states. We notice in this figures that S_n indeed increases with β_2 . For $\beta_2 > 0.70$, the S_n value exceeds the upper limit

of that evaluated in Ref. [66]. Therefore, for the p -wave configuration of the $^{37}\text{Mg}_{gs}$, the deformation parameter remains reasonable even for maximum predicted S_n . On the other hand, with the $^{36}\text{Mg}(0^+) \otimes 2s_{1/2}\nu$ configuration, the S_n remains unchanged with β_2 , which is obvious from Fig. 4(b).

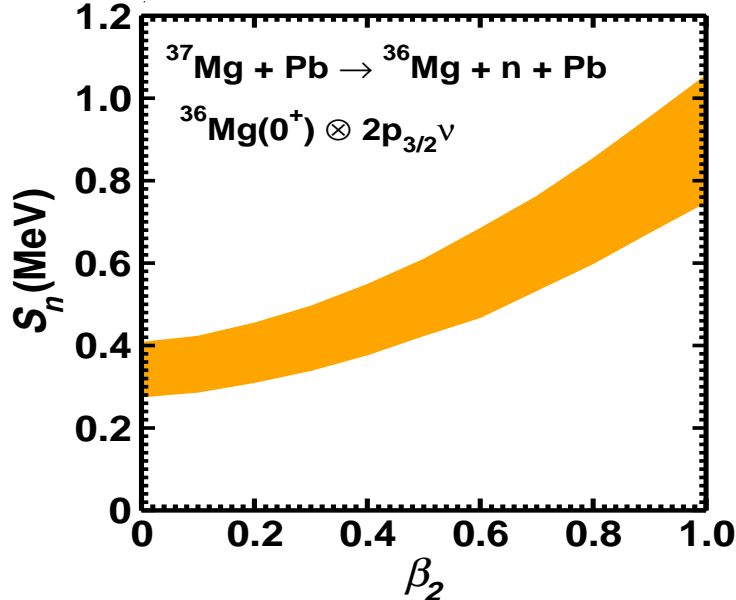


Figure 5: S_n deduced from the comparison of our calculations with the experimental data as a function of the parameter β_2 for the same reaction as in Fig. 4, corresponding to the $^{36}\text{Mg}(0^+) \otimes 2p_{3/2}\nu$ configuration of $^{37}\text{Mg}_{gs}$ with $C^2S = 1.0$.

The investigation of more exclusive observables in the Coulomb breakup reactions of the projectile provides significant advantages in the understanding of its ground state structure. In Fig. 6, we show the $^{36}\text{Mg}-n$ relative energy spectra in Coulomb breakup of ^{37}Mg on a Pb target at the beam energy of 244 MeV/nucleon as a function of the $^{36}\text{Mg}-n$ relative energy (E_{rel}) and β_2 simultaneously. The $^{37}\text{Mg}_{gs}$ configuration is $^{36}\text{Mg}(0^+) \otimes 2p_{3/2}\nu$ with C^2S and S_n values of 1.0 and 0.35 MeV, respectively. We note that the height of the peak depends on the value of β_2 . The position of the peak in this spectrum is dependent on the configuration of the projectile ground state, which is made more explicit in the next figure.

In Fig. 7, we show the relative energy spectra ($d\sigma/dE_{rel}$) as a function of E_{rel} for the same reaction as in Fig. 2 for two different configurations of ^{37}Mg ground state as indicated in the figure. Since, the peak position of

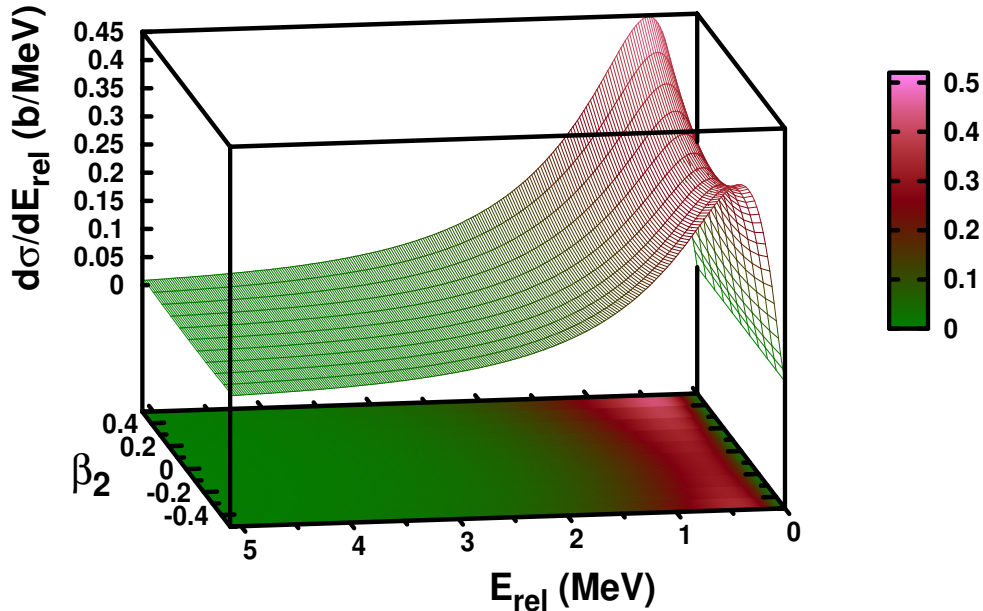


Figure 6: Relative energy spectra for the Coulomb breakup of ^{37}Mg ($J^\pi = 3/2^-$) on a Pb target at 244 MeV/nucleon beam energy, calculated for different values of β_2 with $C^2S = 1.0$ and $S_n = 0.35$ MeV.

$d\sigma/dE_{rel}$ is known to depend on the value of S_n [49, 62, 86, 87], we have used the same values of S_n and C^2S (0.35 MeV and 1.0, respectively), for the two configurations. This ensures that differences seen in the relative energy differential cross sections of the two configurations are attributed solely to the differences in the projectile ground state structure. We see that the relative energy spectra obtained with two configurations show drastically different behavior as a function of E_{rel} . With the s -wave configuration, the magnitude of the cross section near the peak position is more than 3 times larger than that obtained with the p -wave one. Even the peak position of the two configuration are at different values of E_{rel} - the p -wave cross sections peak at higher E_{rel} as compared to those of the s -wave.

In view of the results shown in Fig. 7, measurements of the relative energy spectra in the breakup reactions of ^{37}Mg would be of great help in reducing

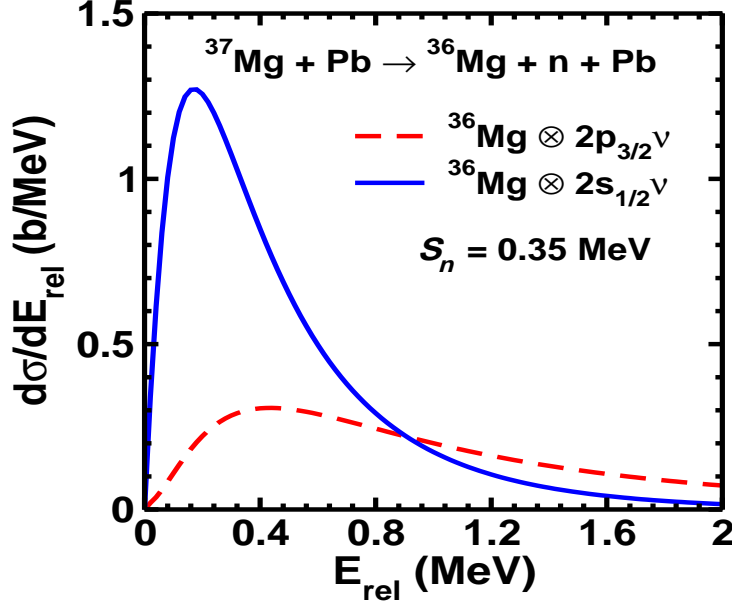


Figure 7: Comparison of relative energy spectra for the Coulomb breakup of ^{37}Mg on Pb target at 244 MeV/nucleon beam energy corresponding to two different possible ground state configurations, $^{36}\text{Mg}(0^+) \otimes 2p_{3/2}\nu$ (dashed line) and $^{36}\text{Mg}(0^+) \otimes 2s_{1/2}\nu$ (solid line). The values of S_n and C^2S are 0.35 MeV and 1.0, respectively for both the configurations. No deformation of the projectile has been included in these calculations.

the uncertainty in its ground state configuration and also in its one-neutron separation energy. Fixing of these quantities will lead to a better understanding of the quadrupole deformation of this nucleus, which also affects the height of the peak in the relative energy spectra.

In Fig. 8, we show the parallel momentum distribution (PMD) of the core fragment ^{36}Mg in the Coulomb breakup reaction $^{37}\text{Mg} + \text{Pb} \rightarrow ^{36}\text{Mg} + \text{n} + \text{Pb}$ at the beam energy of 244 MeV/nucleon. $^{37}\text{Mg}_{gs}$ was assumed to have the $^{36}\text{Mg}(0^+) \otimes 2p_{3/2}\nu$ configuration with S_n and C^2S being 0.35 MeV and 1.0, respectively. Results are shown for several values of the β_2 parameter. We note that the magnitude of the cross section near the peak position is quite sensitive to the β_2 value. Therefore, measurement of this observable is a useful tool for putting constraints on the degree of the quadrupole deformation in ^{37}Mg .

We note from Table 2 that the full width at half maximum (FWHM) of the PMD are almost the same for $\beta_2 \geq 0.30$ (44.0 MeV/c). Even for $\beta_2 =$

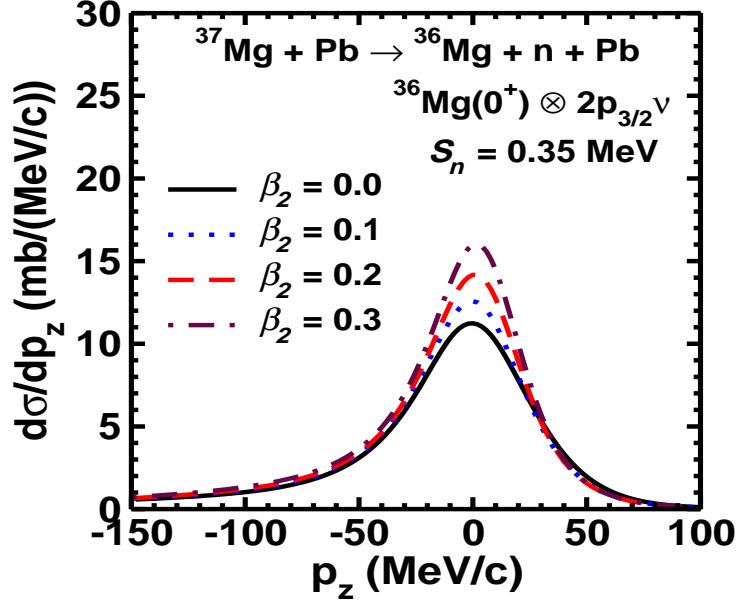


Figure 8: Parallel momentum distribution of ^{36}Mg fragment in the Coulomb breakup of ^{37}Mg on Pb target at 244 MeV/nucleon beam energy for the $J^\pi = 3/2^-$ configuration of $^{37}\text{Mg}_{gs}$ with $S_n = 0.35$ MeV and C^2S of 1.0.

0.0, the FWHM is only about 15% larger than its value at higher β_2 . This is very close to the FWHM of the PMD of the core fragment seen in the breakup reactions of the established low mass halo nuclei like ^{11}Be and ^{19}C . Therefore, the p -wave ($J^\pi = 3/2^-$) ground state of ^{37}Mg is highly likely to have a halo structure.

In Fig. 9, we show a detailed dependence of FWHM of the PMD on the one-neutron separation energy, S_n , for various values of the deformation parameter β_2 . The reactions is the same as that studied in Fig. 8 with the same value of C^2S . We note that regardless of the value of β_2 the FWHM increases with increasing S_n . This is expected because with increasing binding energy the neutron orbits tend to become more and more like those of the nuclei away from the drip line. Furthermore, for most values of S_n , the β_2 dependence of the FWHM of the PMD is similar to that shown in Table 2.

In Fig. 10(a) we show the double differential cross section $d^2\sigma/dE_n d\Omega_n$ as a function of the neutron energy for three neutron angles between $1^\circ - 3^\circ$. The configuration of $^{37}\text{Mg}_{gs}$, and C^2S and S_n values were the same as those in

Table 2: Full width at half maximum of the parallel momentum distribution of ^{36}Mg , obtained in Coulomb breakup of ^{37}Mg on a Pb target at the beam energy of 244 MeV/nucleon. The projectile ground state corresponds to the configuration of $^{36}\text{Mg}(0^+) \otimes 2p_{3/2}\nu$ with S_n and C^2S values of 0.35 MeV and 1.0, respectively.

S_n (MeV)	β_2	FWHM (MeV/c)
0.35	0.0	54.65
	0.1	50.97
	0.2	48.03
	0.3	45.82
	0.4	44.85
	0.5	44.61

Fig. 8. No deformation of the projectile was considered in these calculations (that is $\beta_2 = 0$). We see that magnitude of the cross section near the peak position reduces with increasing neutron angle. An interesting observation is that for all the three angles, the peak occurs near the neutron energy that correspond to the beam velocity. This is consistent with the picture that fragments move with the beam velocity after the breakup. If the charged fragment gets post-accelerated as it leaves the reaction zone (which is the case for the breakup reactions of stable nuclei [75, 76]), one would expect the position of the peak in the neutron spectrum at energies below that corresponding to the beam velocity. We do not see this post-acceleration effect even if Coulomb effects have been included to all orders in the incoming and outgoing channels in our theory. Due to very small binding energies of the halo nuclei and the reactions at higher beam energies, the breakup occurs at distances much larger than the distance of closest approach, thus the post-acceleration effects are minimal [88, 89, 90].

The effect of projectile deformation on the cross section $d^2\sigma/dE_n d\Omega_n$ is studied in Fig. 10(b) for the same reaction as in Fig. 10(a) for one angle of $\theta_n = 1^\circ$. It is evident from this figure that magnitude of the cross section increases with β_2 . This is most visible near the peak position. Therefore, measurements of the double differential cross sections are expected to provide additional information about the deformation of the projectile ground state.

The angular distributions of neutrons emitted in the projectile breakup reactions reflect to a great extent the momentum distribution of the frag-

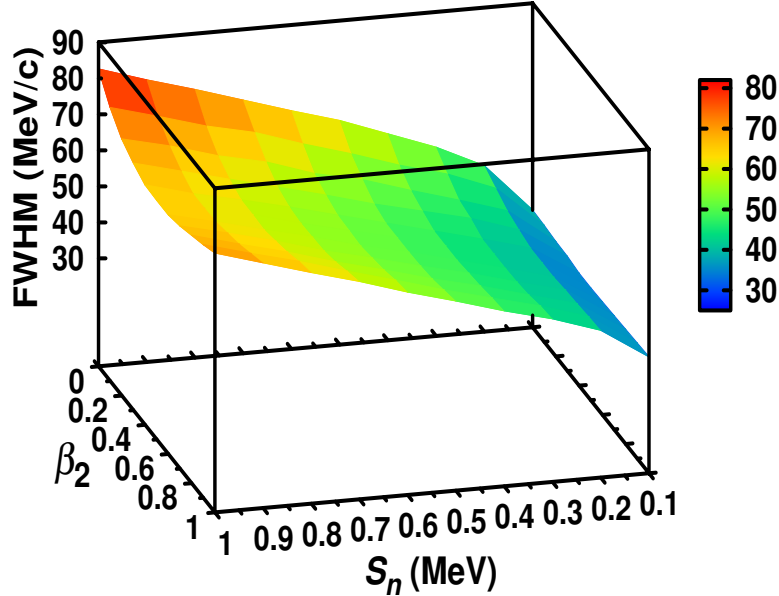


Figure 9: Full width at half maximum of the parallel momentum distribution of ^{36}Mg , obtained in Coulomb breakup of ^{37}Mg on a Pb target at the beam energy of 244 MeV/nucleon as a function of the one-neutron separation energy S_n and the quadrupole deformation parameter β_2 . The projectile ground state corresponds to the configuration of $^{36}\text{Mg}(0^+) \otimes 2p_{3/2}\nu$ with a C^2S value of 1.0.

ments in the ground state of the projectile (see, e.g., Ref. [91]). Therefore, their study is expected to provide further information about the neutron halo structure in ^{37}Mg . In Fig. 11, we show the neutron angular distribution in the Coulomb breakup reaction $^{37}\text{Mg} + \text{Pb} \rightarrow ^{36}\text{Mg} + n + \text{Pb}$ at the beam energy of 244 MeV/nucleon. The ground state configuration, the S_n and C^2S were the same as those in Fig. 10. The results are presented for four values of the β_2 parameter. We notice that cross sections drop very steeply with increasing neutron angle in the forward directions. The narrow angular distributions of neutrons below the grazing angles in the Coulomb breakup reactions of ^{37}Mg reflect the small widths of the parallel momentum distribution and hence the large spatial extension of the valence neutron in its ground state. The effect of the deformation is significant at the forward angles [this was already seen in Fig. 10(b)].

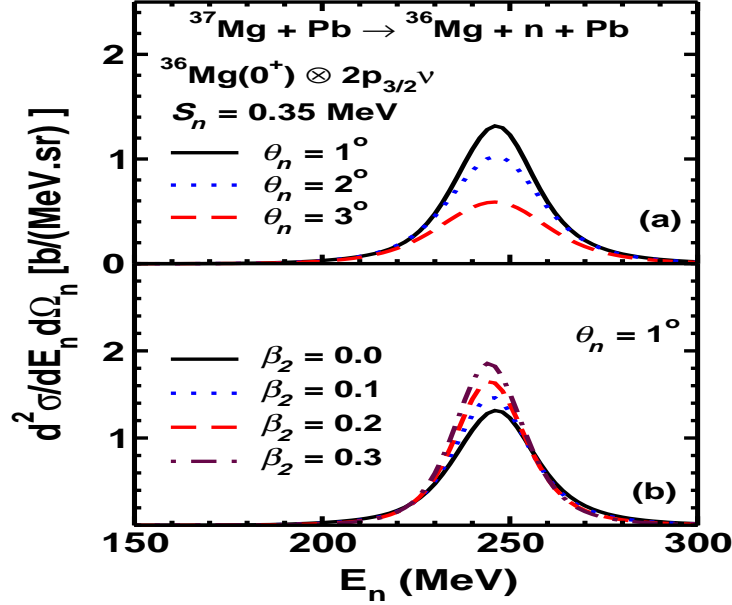


Figure 10: Neutron energy-angular distribution for the Coulomb breakup of ^{37}Mg on a Pb target at 244 MeV/nucleon beam energy calculated for $S_n = 0.35$ MeV and $C^2S = 1.0$ for the projectile ground state configuration corresponding to $J^\pi = 3/2^-$ for (a) (θ_n) at 1° , 2° and 3° , and (b) with different values of β_2 for $\theta_n = 1^\circ$,

4. Summary and Conclusions

In this paper we have studied the Coulomb breakup reaction $^{37}\text{Mg} + \text{Pb} \rightarrow ^{36}\text{Mg} + \text{n} + \text{Pb}$ at the beam energy of 244 MeV/nucleon, within the framework of the post form finite range distorted wave Born approximation theory that is extended to include the projectile deformation effects. In this formalism the transition amplitude is factorized into two parts - one containing the dynamics of the reaction and the another the projectile structure informations such as the fragment-fragment interaction and the corresponding wave function in its ground state. Analytic expressions can be written for both parts. This formalism opens up a route to perform realistic quantum mechanical calculations for the breakup of neutron-drip line nuclei in the medium mass region that can be deformed.

We calculated the total one-neutron removal cross sections (σ_{-1n}) in this reaction and compared our results with the corresponding data reported in a recent publication [23] in order to determine the configuration of the ^{37}Mg ground state. The analysis of this single measured cross section already

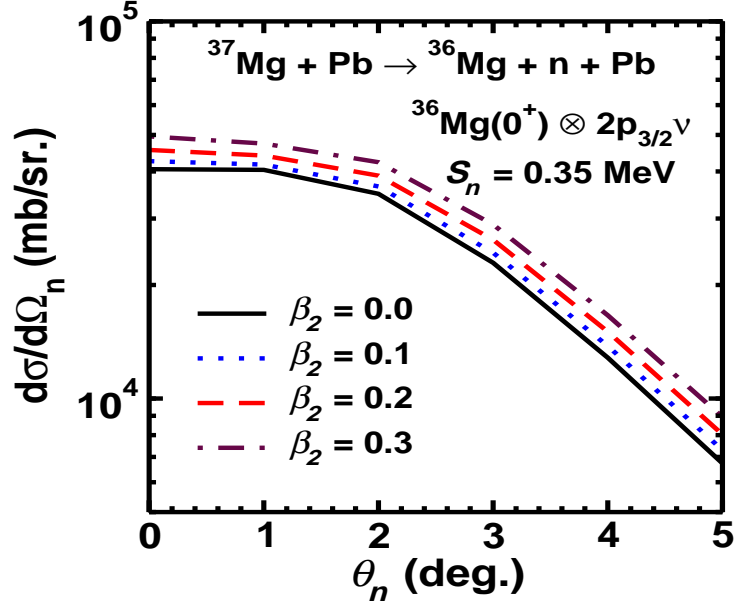


Figure 11: Neutron angular distribution for Coulomb breakup of ^{37}Mg on a Pb target at 244 MeV/nucleon beam energy. The projectile ground state configuration, S_n and C^2S were the same as those in Fig. 10.

rules out the $^{36}\text{Mg}(0^+) \otimes 1f_{7/2}\nu$ configuration for the ground state of ^{37}Mg . However, it does not allow to exclude either of the $^{36}\text{Mg}(0^+) \otimes 2p_{3/2}\nu$ and $^{36}\text{Mg}(0^+) \otimes 2s_{1/2}\nu$ configurations for $^{37}\text{Mg}_{gs}$. Assuming a spectroscopic factor of one, the extracted values of one-neutron separation energies for these two configurations are 0.35 ± 0.06 MeV and 0.50 ± 0.07 MeV, respectively. However, the deduced S_n depends on the value of C^2S . Our study shows that S_n rises steadily with increasing C^2S .

In order to gain more insight in the ground state structure of ^{37}Mg , we studied the effect of the projectile deformation on σ_{-1n} . We find that for the configuration $^{36}\text{Mg}(0^+) \otimes 2p_{3/2}\nu$ for the ^{37}Mg ground state, the calculated σ_{-1n} overlaps with the experimental data band for the quadrupole deformation parameter (β_2) below 0.32. This is in line with the Nilsson model calculations of Ref. [37] where the β_2 for this state is predicted to lie in the range 0.30 - 0.34. However, with the $^{36}\text{Mg}(0^+) \otimes 2s_{1/2}\nu$ configuration, the overlap between calculations and the data occurs for even very large values of β_2 . Thus with this configuration, our calculations are unable to put any constraint on deformation parameter β_2 .

We also calculated more exclusive observables such as the core-valence neutron relative energy spectra, the energy-angle and the angular distributions of the emitted neutron and the parallel momentum distribution of the core fragment. The position of the peak as well as the magnitude of the cross section near the peak of the core-valence neutron relative energy spectra are found to be dependent on the configuration of the projectile ground state as well as on its deformation. Similar trend was also observed in the parallel momentum distribution of the core fragment. The FWHM of this distribution are found to be of the same order of magnitude as those seen in the breakup of established light halo nuclei. This confirms that ^{37}Mg ground state has a halo structure. The angular distribution of the emitted neutrons is strongly forward peaked and the cross sections in the forward directions, are dependent on the projectile deformation. Thus, we identified the observables that are more critically dependent on the ground state structure of the projectile. Therefore, our study is expected to provide motivation for future experiments on breakup reactions of the neutron rich medium mass nuclei.

In calculations of the breakup reactions of nuclei at higher beam energies, relativistic effects could play a role [92, 93]. Our theory is essentially non-relativistic in nature. Nevertheless, we have seen in Ref. [54] that this theory is able to reproduce well the data on the excitation energy spectra and the total electromagnetic one-neutron removal cross section in the breakup reaction of ^{23}O on a Pb target at even higher beam energy of 422 MeV/nucleon. In the present study we did check that inclusion of relativistic effects at the kinematics level does not have any significant effect on the cross sections. A fully relativistic dynamical quantal theory of breakup reactions is still not available.

Acknowledgments

This work has been supported by the Department of Science and Technology of the Government of India, under the grant number SR/S2/HEP-040/2012. One of the authors (RS) is supported by the Council of Scientific and Industrial Research (CSIR), India. KT is supported by the Brazilian Ministry of Science, Technology and Innovation (MCTI-Brazil), and Conselho Nacional de Desenvolvimento Científico e Tecnológico (CNPq).

References

- [1] C. Thibault *et al.*, Phys. Rev. C **12** (1975) 644.
- [2] C. Huber *et al.*, Phys. Rev. C **18** (1978) 2342.

- [3] C. Detraz *et al.*, Phys. Rev. C **19** (1979) 164.
- [4] D. Guillemaud-Mueller *et al.*, Nucl. Phys. **A426** (1984) 37.
- [5] P. Baumann *et al.*, Phys. Lett. **B228** (1989) 458.
- [6] T. Motobayashi *et al.*, Phys. Lett. **B346** (1995) 9.
- [7] B. V. Pritychenko *et al.*, Phys. Rev. C **63** (2000) 011305.
- [8] H. Iwasacki *et al.*, Phys. Lett. **B522** (2001) 9.
- [9] Y. Yanagisawa *et al.*, Phys. Lett. **566** (2003) 84.
- [10] J. A. Church *et al.*, Phys. Rev. C **72** (2005) 054320.
- [11] G. Neyens *et al.*, Phys. Rev. Lett. **94** (2005) 022501.
- [12] D. T. Yordanov *et al.*, Phys. Rev. Lett. **99** (2007) 212501.
- [13] A. Gade *et al.*, Phys. Rev. Lett. **99** (2007) 072502.
- [14] P. Himpe *et al.*, Phys. Lett. **B658** (2008) 203.
- [15] O. Sorlin and M.-G. Porquet, Prog. Part. & Nucl. Phys. **61** (2008) 602.
- [16] P. Doornenbal, *et al.*, Phys. Rev. Lett. **103** (2009) 032501.
- [17] R. Kanungo *et al.*, Phys. Lett. Phys. Lett. **B 685** (2010) 253.
- [18] K. Wimmer *et al.*, Phys. Rev. Lett. **105** (2010) 252501.
- [19] N. Hinohara *et al.*, Phys. Rev. C **84** (2011) 061302.
- [20] A. Gade *et al.*, Phys. Rev. C **83** (2011) 044305.
- [21] P. Doornenbal, *et al.*, Phys. Rev. Lett. **111** (2013) 212502.
- [22] T. Nakamura, *et al.*, Phys. Rev. Lett. **103** (2009) 262501.
- [23] N. Kobayashi *et al.*, Phys. Rev. Lett. **112** (2014) 242501.
- [24] O. Haxel, J. Jensen, and H. Suess, Phys. Rev. **75** (1949) 1766.
- [25] M. G. Mayer, Phys. Rev. **75** (1949) 1969.

- [26] E. K. Warburton, J. A. Becker and B. A. Brown, Phys. Rev. C **41** (1990) 1147.
- [27] H. Iwasaki *et al.*, Phys. Lett. B **481** (2000) 7.
- [28] B. Bastin *et al.*, Phys. Rev. Lett. **99** (2007) 022503.
- [29] N. Orr *et al.*, Phys. Lett. **B258** (1991) 29.
- [30] T. Otsuka *et al.*, Phys. Rev. Lett. **95** (2005) 232502.
- [31] K. Yoneda *et al.*, Phys. Lett. **B 499** (2001) 233.
- [32] X. Campi, H. Flocard, A. K. Kerman, and S. Koonin, Nucl. Phys. **A251** (1975) 193.
- [33] S. K. Patra and C. R. Praharaaj, Phys. Lett. **B 273** (1991) 13.
- [34] A. Poves and J. Retamosa, Nucl. Phys. **A571** (1994) 221.
- [35] Y. Utsuno, T. Otsuka, T. Mizusaki, and M. Honma, Phys. Rev. C **60** (1999) 054315.
- [36] T. Otsuka, R. Fujimoto, Y. Utsuno, B. A. Brown, M. Honma, and T. Mizusaki, Phys. Rev. Lett. **87** (2001) 082502.
- [37] I. Hamamoto, Phys. Rev. C **76** (2007) 054319.
- [38] I. Hamamoto, Phys. Rev. C **85** (2012) 064329.
- [39] M. Takechi *et al.*, Nucl. Phys. **A 834** (2010) 412c.
- [40] M. Takechi *et al.*, Phys. Lett. **B 707** (2012) 357.
- [41] M. Takechi *et al.*, EPJ Web of Confs. **66** (2014) 02101.
- [42] K. Minoto, T. Sumi, M. Kimura, K. Ogata, Y. R. Shimizu, and M. Yahiro, Phys. Rev. Lett. **108** (2012) 052503.
- [43] T. Sumi, K. Minoto, S. Tagami, M. Kimura, T. Matsumoto, K. Ogata, Y. R. Shimizu, and M. Yahiro, Phys. Rev. C **85** (2012) 064613.
- [44] W. Horiuchi, T. Inakura, T. Nakatsukasa, and Y. Suzuki, Phys. Rev. C **86** (2012) 024614.

- [45] S. Watanabe *et al.*, Phys. Rev. C **89** (2014) 044610.
- [46] I. Tanihata *et al.*, Phys. Rev. Lett. **55** (1985) 2676.
- [47] G. Hansen and B. Jonson, Europhys. Lett. **4** (1987) 409.
- [48] C. A. Bertulani, L. F. Canto and M. S. Hussein, Phys. Rep. **226** (1993) 281.
- [49] P. Banerjee and R. Shyam, Phys. Rev. C **61** (1999) 047301.
- [50] B. Jonson, Phys. Rep. **389** (2004) 1.
- [51] T. Frederico, A. Dalfino, L. Tomio, and M. Yamashita, Prog. Part. Nucl. Phys. **67** (2012) 939.
- [52] I. Tanihata, H. Savajols, and R. Kanungo, Prog. Part. Nucl. Phys. **68** (2013) 215.
- [53] V. Rotival and T. Duguet, Phys. Rev. C **79** (2009) 054308.
- [54] R. Chatterjee, R. Shyam, K. Tsushima and A. W. Thomas, Nucl. Phys. **A913** (2013) 116.
- [55] B. Jurado *et al.*, Phys. Lett. **101** (2007) 023210.
- [56] L. Gaudefroy *et al.*, Phys. Rev. Lett. **109** (2012) 202503.
- [57] T. Nakamura *et al.*, Phys. Lett. **B331** (1994) 296.
- [58] F. M. Nunes, I. J. Thompson and R. C. Johnson, Nucl. Phys. **A 596**, (1996) 171.
- [59] T. Aumann *et al.*, Phys. Rev. Lett. **84** (2000) 35.
- [60] R. Palit *et al.*, Phys. Rec. C **68** (2003) 034318.
- [61] T. Nakamura *et al.*, Phys. Rev. Lett. **83** (1999) 1112.
- [62] G. Baur, K. Hencken and D. Trautmann, Prog. Part. Nucl. Phys. **51** (2003) 487.
- [63] R. Chatterjee, P. Banerjee and R. Shyam, Nucl. Phys. A **675** (2000) 477.

- [64] Shubhchintak and R. Chatterjee, Nucl. Phys. A **922** (2014) 99.
- [65] T. Nakamura *et al.*, Phys. Rev. Lett. **112** (2014) 142501.
- [66] M. Wang, G. Audi, A.H. Wapstra, F.G. Kondev, M. MacCormick, X. Xu, and B. Pfeiffer, Chin. Phys. C **36** (2012) 1603.
- [67] M. Terasawa, K. Sumiyoshi, T. Kajino, G. J. Mathews, and I. Tanihata, Astr. J. **562** (2001) 470.
- [68] A. Deltuva and A. C. Fonseca, Phys. Rev. C **79** (2009) 014606.
- [69] R. Crespo, A. Deltuva, M. Rodriguez-Gallardo, E. Cravo and A. C. Fonseca, Phys. Rev. C **79** (2009) 014609.
- [70] E. Cravo, R. Crespo, A. M. Moro and A. Deltuva, Phys. Rev. C **81** (2010) 031601.
- [71] N. J. Upadhyay, A. Deltuva and F. M. Nunes, Phys. Rev. C **85** (2012) 054621.
- [72] G. R. Satchler, *Direct Nuclear Reactions*, (Oxford University Press, New York, 1983).
- [73] N. Austern, *Direct Nuclear Reactions Theory*, (Wiley, New York, 1970).
- [74] N. Glendenning, *Direct Nuclear Reaction*, (Academic 1983).
- [75] G. Baur and D. Trautmann, Nucl. Phys. A **A191** (1972) 321.
- [76] G. Baur, F. Rösler, D. Trautmann, and R. Shyam, Phys. Rep. **111**, (1984) 333.
- [77] R. Shyam and P. Danielewicz, Phys. Rev. C **63** (2001) 054608.
- [78] P. Braun-Munzinger and H.L. Harney, Nucl. Phys. **A233** (1974) 381.
- [79] R. Shyam and M. A. Nagarajan, Ann. Phys. (N.Y.) **163** (1985) 265.
- [80] A. Nordsieck, Phys. Rev. **93** (1954) 785.
- [81] I. Hamamoto, Phys. Rev. C **69** (2004) 041306(R).
- [82] G. Fäldt and R. Glauber, Phys. Rev. C **42** (1990) 395.

- [83] M. Moshinsky, Nucl. Phys. **13** (1959) 104.
- [84] P. G. Hansen and J. A. Tostevin, Annu. Rev. Nucl. Part. Sci. **53** (2003) 219 and references therein.
- [85] A Watt, R P Singhal, M H Storm and R R Whitehead, J. Phys. G **7** (1981) L145.
- [86] M. A. Nagarajan, S. Lenzi and A. Vitturi, Eur. Phys. J. A **35** (2005) 63.
- [87] S. Typel and G. Baur, Nucl. Phys. A **759** (2005) 247.
- [88] P. Banerjee and R. Shyam, Nucl. Phys. A **561** (1993) 112.
- [89] P. Banerjee and R. Shyam, J. Phys. G: Nucl. Part. Phys. **22** (1996) L79.
- [90] P. Banerjee, G. Baur, K. Hencken, R. Shyam and D. Trautman, Phys. Rev. C **65** (2002) 064602.
- [91] H. Esbensen, Phys. Rev. C **44** (1991) 440.
- [92] C. A. Bertulani, Phys. Rev. Lett. **94** (2005) 072701.
- [93] K. Ogata, C. A. Bertulani, Progr. Theor. Phys. **121** (2009) 1399.